Effect of filler on performance of porous asphalt pavement using multiscale finite element method

Du, Cong; Lu, Guoyang; Wang, Haopeng; Sun, Yiren; Liu, Pengfei; Wang, Dawei; Leischner, Sabine ; Oeser, Markus

DOI
10.1080/10298436.2021.1888090

Publication date
2021

Document Version
Accepted author manuscript

Published in
International Journal of Pavement Engineering

Citation (APA)
Du, C., Lu, G., Wang, H., Sun, Y., Liu, P., Wang, D., Leischner, S., & Oeser, M. (2021). Effect of filler on performance of porous asphalt pavement using multiscale finite element method. *International Journal of Pavement Engineering*, *23*(9), 3244-3254. https://doi.org/10.1080/10298436.2021.1888090

Effect of filler on performance of porous asphalt pavement using multiscale finite element method

Abstract: Porous asphalt (PA) pavements are widely employed in areas with wet climates due to their excellent permeability and superior performance. As particle enhancement inclusions in asphalt mastic, mineral fillers play essential roles in improving the performance of PA pavements. This study developed a coupled multiscale finite element (FE) model, involving the mesostructure of PA mixture and PA pavement. Within this model, the mesoscale structure was captured by X-ray computer tomography (X-ray CT) scanning and reconstructed with digital image processing (DIP) technology. Four types of mastic properties were employed with four mineral fillers (Granodiorite, Limestone, Dolomite, and Rhyolite) in the mesoscale portion of the pavement model to analyze the effects of filler types on the performance of pavements. A constant tire loading was applied and two temperatures (0 °C and 50 °C) were specified. The performances (load-bearing capacity, rutting resistance, and raveling resistance) of pavements with different fillers were identified and ranked, and their correlations with the chemical components of the four fillers were analyzed. The computational results showed that pavements with Rhyolite and Granodiorite fillers have higher load-bearing capacities and rutting resistance, while the Limestone and Dolomite fillers can improve the raveling resistance of the PA pavements. In the correlation analysis, the chemical components Al_2O_3 and SiO_2 play dominant roles in improving the load-bearing capacities and rutting resistance of the PA pavements, and the fillers with high percentages of CaO can improve the raveling resistance of the PA pavements. Based on this algorithm, it is possible to select an optimal filler for a specific pavement design and thus improve the durability of the PA pavements.

Keywords: porous asphalt pavement; multiscale finite element model; mineral filler; correlation analysis; chemical components

1. Introduction

Due to its superior ability to improve driving safety during wet weather, porous asphalt (PA) is broadly used as an innovative surfacing technology throughout the world. The open structure of PA exhibits excellent performance in allowing water to permeate from the surface as well as reducing noise from highway traffic, and hence improving riding quality and visibility especially in wet conditions (Alber *et al.* 2018, Lu *et al.* 2019a, Lu *et al.* 2019b). However, the high percentage of air void content significantly affects the strength of the PA layers, and hence, the stresses generated by traffic loads have a profound effect on the durability of PA pavements. Moreover, the open structures make it difficult to deeply investigate the mechanical performance of PA pavements. The mechanical performance of PA mixture is not only related to the fundamental material properties, but also its geometric feature at mesoscale (Mohd Shukry *et al.* 2018, Qian *et al.* 2020). Improving the understanding of the mechanism of PA can significantly promote the structural design approach, and a long-life higher performance pavement infrastructure can therefore be established.

The addition of mineral filler is wildly employed as a common practice to enhance the performance-related properties of asphaltic materials. Research has proved that the filler plays a dual role in asphalt mixtures, which respectively are that of particle enhancement inclusion and active interfacial material (Kim and Little 2004, Cardone *et al.* 2015). In particular, for PA, in which the strength is provided mainly by coarse aggregate interaction, fillers play an essential role in increasing the viscosity of the asphalt mastic for binding the coarse aggregates and preventing the movement of aggregate particles. To date, numerous experimental studies have been conducted to

investigate the effects of the mineral fillers on the mechanical and damage properties of the asphalt mastic and mixtures. Rochlani *et al.* (2019) investigated and compared the rheology properties as well as the fatigue, rutting, and low-temperature cracking susceptibility of bitumen with four different filler types (dolomite, granodiorite, limestone, and rhyolite). Rieksts *et al.* (2018) conducted the dynamic shear rheometer (DSR) test on the mastic with three different mineral fillers; the experimental results provide the mastic performance in terms of permanent deformations. In terms of the surface free energy, Alvarez *et al.* (2019) assessed the effect of fillers on the response of asphalt-aggregate interfaces, and the results led to a recommendation of an optimum range of filler volumetric concentrations. In addition, the effects of fillers on the fracture and fatigue properties of the asphalt mastic and asphalt mixture were also investigated by scholars (Al-Hdabi *et al.* 2014, Fonseca *et al.* 2019, Stewart and Garcia 2019, Roberto *et al.* 2020). As mentioned above, the mineral fillers can enhance the performance of asphalt mastic and mixture, and the effects of the fillers are significantly influenced by their types, volume concentrations, and gradations.

However, numerical studies focusing on the mechanical performance of the PA mixtures and PA pavements influenced by different fillers are seldom published in the literature. In the past, numerical studies regarded the multi-phase asphalt mixture, including bitumen, fillers and aggregates, as a homogeneous material due to the limitation of computation capacity. In fact, the influence of the heterogeneous feature of asphalt mixtures is non-negligible, especially for the PA mixtures in which the air void content is greater than 10% (Alvarez *et al.* 2011, Liu *et al.* 2011, Liu *et al.* 2012). Thus, investigations on the mesoscale structure of PA mixtures can provide a deep insight into the stress-strain relations in pavement.

Currently, two approaches are employed to establish the mesoscale models of

multiphase composites: random generation algorithm and digital image processing (DIP) technology. Random generation is regarded as the efficient method without extensive labor work. Based on the random take-and-place method, polygon inclusions with various shapes, locations, and orientations can be specified and distributed around the matrix (Liu *et al.* 2018b). Therefore, it is very convenient for scholars to establish the multi-phase models for numerical simulations. Researches have employed this approach to investigate the mechanical behavior of asphalt mixture at mesoscale. For example, Wang *et al.* (2014) analyzed the fracture performance of asphalt mixture using the randomly generated two-dimensional (2D) microstructure models, in which the cohesive zone model (CZM) theory and extensive finite element method (XFEM) were utilized to represent the crack initiations. In conjunction with the CZM, Yin *et al.* (2012) investigated the tensile strength of asphalt mixture based on the heterogeneous model developed with the combination of the aggregate generation and packing algorithm.

However, the inner structure of asphalt mixture closely relies on the laboratory mixing and compacting process, and thus the random generation models are untenable to represent the aggregate distribution and orientations at mesoscale. To address this issue, the DIP method is based on the digital image of specimens, and can establish the mesoscale structure of the real asphalt mixture. Afterwards, finite element methods (FEM) (Dai *et al.* 2005, Liu *et al.* 2018a, Kollmann *et al.* 2019, Sun *et al.* 2019, Sun *et al.* 2020) and discrete element methods (DEM) (Li *et al.* 2019, Zhang *et al.* 2019) can be incorporated to calculate the mesoscale mechanics of the asphalt mixture.

Nonetheless, an asphalt pavement containing many inclusions, voids, and micro cracks would require a large amount of mesh element. Therefore, it is unrealistic to conduct a time-consuming and device-related mesoscale simulation on the entire asphalt pavement. As a remedy, an innovative approach in which both the mesoscale structure

of asphalt mixture and the macroscale structure of asphalt pavement can be simultaneously modeled is the finite element (FE) simulation (Ziaei-Rad *et al.* 2012, Zhang and Leng 2017, Du *et al.* 2020, Klimczak and Cecot 2020, Wollny *et al.* 2020). The impact of crumb rubber on the improvement of PA mixtures was studied by comparison with a control mixture using the FE method. It was found that static loading resulted in slightly greater rut depth than the repeated loading, and an increase of the rubber content caused less rut depth (Imaninasab *et al.* 2016). 2D FE modelling was used to evaluate the potential contribution of PA layers with different thicknesses to the overall structural capacity of different flexible pavements. The results showed that PA layers did contribute to the pavements' structural capacity and this contribution strongly depended on their different microstructural and geometric characteristics (Manrique-Sanchez and Caro 2019). Within this configuration, the mechanical response of asphalt pavement can be precisely demonstrated while considering the details of the inner structure of asphalt mixture.

To investigate the influence of the different mineral fillers on the mechanical performance of the PA pavement, a coupled multiscale FE model was established for this study in the FE software ABAQUS. The mesoscale structure model of the PA mixture was created based on the CT scanning image, and the mesoscale model was coupled into a macroscale structure of asphalt pavement. Within the mesoscale model, four types of asphalt mastic were employed that each contained different types of mineral fillers: Granodiorite, Limestone, Dolomite, and Rhyolite. A constant tire loading was applied on the mesoscale region, and the mechanical responses were investigated to demonstrate the effects of the filler types on the performance of the PA pavement.

2. Methodology

2.1. Preparation of the porous asphalt samples

The PA used in this study was a common type with a maximum grain size of 8 mm following the German standard ZTV Asphalt-StB 07 (2007). The specimen was mixed of crushed diabase aggregates, mineral filler, and bitumen with a 50/70 penetration grade. The detailed mix design is listed in **Table 1**. The PA samples were prepared by a Marshall compactor with 50 impacts per side (Rochlani *et al.* 2019).

Table 1. Mix design of porous asphalt

Component	Grain size (mm)	Mass percentage (%)	Air void content (Vol.-%)
Mineral filler	0-0.063	5.0	-
	0.063-2	15.0	-
Diabase	2-5.6	37.0	-
	5.6-8	43.0	-
Mixture	-	-	26.2

A previous study (Rochlani *et al.* 2019) has investigated the chemical compositions of the four types of mineral filler, which are listed in **Table 2**.

Table 2. Chemical composition of mineral filler

	Na_2O	MgO	Al_2O_3	SiO_2	K_2O	CaO	TiO_2	Fe_2O_3	others
Granodiorite	3.22	2.44	18.09	61.70	3.42	2.73	1.04	6.35	0.58
Limestone	0.18	2.02	1.29	1.94	0.19	92.97	0.12	0.82	0.46
Dolomite	0.27	26.02	2.26	5.23	0.61	61.97	0.07	1.91	1.60
Rhyolite	1.42	0.41	19.65	65.69	8.98	0.26	0.26	3.04	0.24

Notice that the microstructures of the PA with different types of mineral filler are identical. Therefore, the limestone filler was selected to prepare the PA mixture specimen in order to identify its microstructure. Subsequently, the mastics respectively with the four types of mineral filler were prepared with a binder-filler mass ratio of 1:1.6. This value was chosen to mimic the binder-filler ratio of a stone mastic asphalt, SMA 11S, which is the most popular asphalt mixture used in Germany. Their rheological properties were determined by strain and frequency sweep tests (Rochlani *et al.* 2019).

2.2. Viscoelastic properties of asphalt mastic

In the finite element simulation, the basic hereditary integral formulation for the rate-dependent viscoelastic materials can be presented as (Schapery 1981),

$$\sigma(t)=\int_0^t E(t\text{-}\tau)\frac{\mathrm{d}\varepsilon(\tau)}{\mathrm{d}\tau}\mathrm{d}\tau \tag{1}$$

where $\sigma(t)$ and $\varepsilon(t)$ are the stress and strain, respectively; $E(t)$ is the modulus; t is the reduced time, which is related to the temperature shift function. In this study, different viscoelastic parameters under different temperatures were provided, and hence t denotes the actual time.

The Prony series is widely employed to characterize the viscoelastic properties in finite element simulations, which can be presented by the generalized Maxwell model (Tschoegl 2012, Shafabakhsh *et al.* 2018). The rete-dependent modulus can be formulated as,

$$E(t)=E_\infty+\sum_{i=1}^{N}E_i e^{-t/\rho_i} \tag{2}$$

where E_∞ is the equilibrium modulus; E_i and ρ_i are the i-th relaxation strength and relaxation time, respectively; N is the number of the Maxwell elements. In practice, the parameters of the Prony series for asphalt mastic can be determined according to the frequency sweep tests by the Dynamic Shear Rheometer (DSR) (Rochlani *et al.* 2019).

2.3. Development of the coupled multiscale model

As aforementioned, the mesoscale structure of the PA was established based on the digital CT image of the specimen. In terms of the DIP technology, the CT image was first converted to the binary one according to its intensity values. Thus the areas of the air voids and aggregates could be separately identified. Subsequently, the coordinates of the vertex of polygonal aggregates and air voids could be determined by incorporating

the boundary detection and polygon approximation technologies (Reyes-Ortiz *et al.* 2019, Xing *et al.* 2019). In this study, the air voids with size larger than 1 mm could be effectively identified by the DIP technology and be reconstructed in the FE model. While the air voids smaller than 1 mm were considered as part of the asphalt mastic because the total content of such air voids is relatively small and the influence on the mechanical properties of the asphalt mastic can be neglected (Zhang *et al.* 2016). Consequently, the mesoscale model of the PA mixture was established in the axisymmetric coordinates based on the parametric modeling method of ABAQUS, which can afford comparable simulation accuracy to the three-dimensional model as well as significantly save the computational time. The mesoscale model was discretized by CAX3 (3-node linear axisymmetric element) and CAX4 (4-node bilinear axisymmetric element), as shown in **Figure 1**.

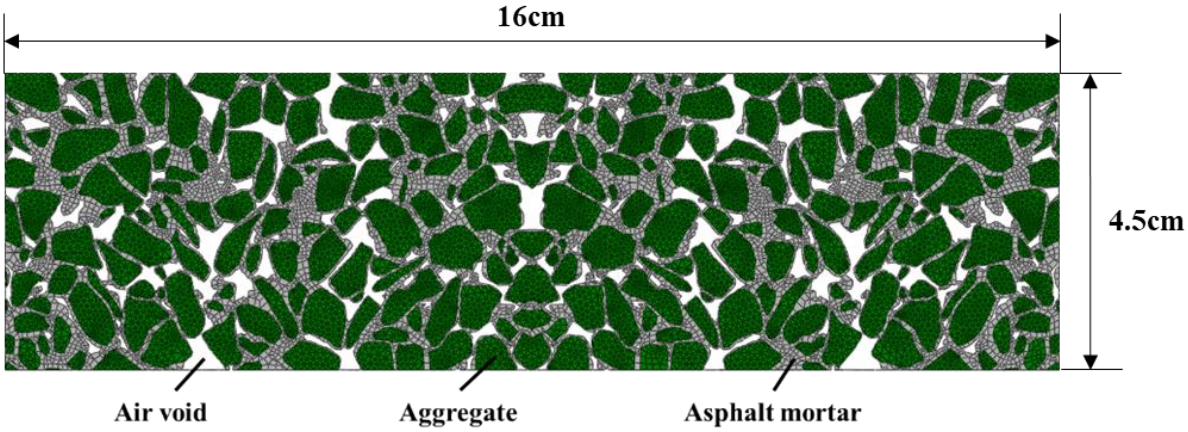

Figure 1 Image of the mesoscale model of porous asphalt mixture

According to the German pavement design specification (2015), the macroscale FE model of PA pavement was developed in the axisymmetric coordinate system, and the loading area was defined as a circular region with a radius of 10cm at center. The macroscale model was discretized by CAX4 elements. The symmetry axis and bottom of the model were respectively restricted in the horizontal and vertical directions. Due to

the limitation of the size of the CT image, the mesoscale part of asphalt pavement was selected at the center of the surface layer with a size of 16 cm × 4.5 cm. To precisely characterize the mechanical performance of the PA mixture, the fine mesh elements with a size of 1 mm were employed in the mesoscale part. In addition, to save computation time, the coarser elements with sizes ranging from 1 mm to 50 mm were used away from the mesoscale part in the model. This setup of the mesh size was based on a comprehensive mesh study. The coupled multiscale model is presented in **Figure 2**.

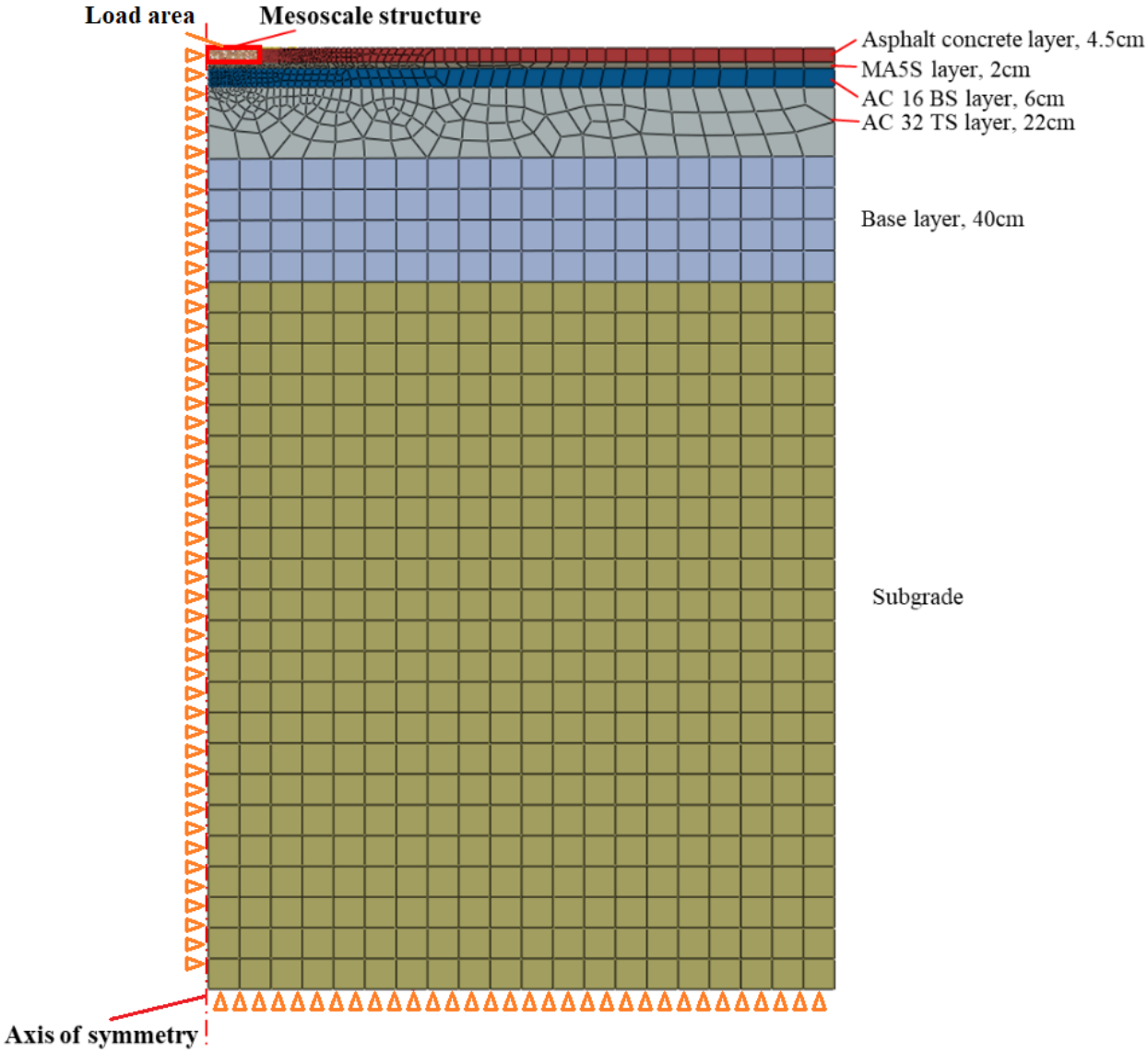

Figure 2 Image of the multiscale model of asphalt pavement

Table 3 lists the model parameters for the mesoscale part, i.e., asphalt mastic and

aggregate. In this study, the viscoelastic properties of the asphalt mastics were used to define the model parameters for the asphalt mortar. The Prony series at 0 °C and 50 °C, which are the classic linear viscoelastic parameters in FE simulation, was specified in the asphalt mastic to represent the time-dependent performance according to a previous study (Rochlani *et al.* 2019). The Young's modulus and Poisson's ratio of aggregate were assigned in terms of the work from (Kim *et al.* 2012). **Table 4** lists the parameters for the macroscale part. The linear elastic Young's modulus of the base layer and subgrade were defined in terms of typical values (Sun *et al.* 2019). In addition, the elastic modulus of the MA5S layer, AC 16 BS layer, and AC 32 TS layer were assigned as temperature-dependent (Liu *et al.* 2017). For the time-dependent elastic properties of PA layers with different mineral fillers, the Young's modulus and Poisson's ratio were identified based on the calculation of the macro-mechanical responses of the mesoscale model (Allen 2001).

Table 3 Model parameters for mesoscale model

Series	Mastic_Granodiorite				Mastic_Limestone			
	0 °C		50 °C		0 °C		50 °C	
i	ρ_i	E_i(MPa)	ρ_i	E_i(M Pa)	ρ_i	E_i(MPa)	ρ_i	E_i(MPa)
1	7.08E+09	2.34E-03	6.47E+08	9.24E-03	5.25E+05	1.03E+01	8.84E+02	6.89E-03
2	9.05E+05	2.73E+01	1.23E+09	2.39E-03	1.00E+00	1.48E+02	1.05E+03	1.67E-03
3	7.08E+09	2.96E-01	4.57E+08	5.23E-04	8.25E+07	1.01E-02	9.30E+02	6.87E-04
4	1.00E+00	2.30E+02	6.64E+08	1.29E-04	7.00E+09	7.33E-02	9.26E+02	4.93E-04
5	3.16E-07	7.07E+03	3.16E-07	2.00E+03	3.16E-07	7.00E+03	3.16E-07	1.42E+02
6	3.16E-06	3.02E+03	3.16E-06	3.10E+01	3.16E-06	3.85E+03	3.16E-06	1.37E+02
7	3.16E-05	1.19E+03	3.16E-05	4.34E+01	3.16E-05	1.34E+03	3.16E-05	3.19E+01
8	3.16E-04	6.65E+02	3.16E-04	1.44E+01	3.16E-04	6.24E+02	3.16E-04	1.04E+01
9	3.16E-03	5.44E+02	3.16E-03	3.32E+00	3.16E-03	4.62E+02	3.16E-03	2.03E+00
Series	Mastic_Dolomite				Mastic_Rhyolite			
	0 °C		50°C		0 °C		50 °C	
i	ρ_i	E_i(MPa)	ρ_i	E_i(MPa)	ρ_i	E_i(MPa)	ρ_i	E_i(MPa)
1	5.55E+09	2.15E+00	5.13E+03	1.12E-02	5.02E+09	8.38E-03	1.32E+09	1.75E-02
2	1.18E+09	2.14E+00	5.22E+03	3.37E-04	4.99E+09	1.18E-02	1.56E+09	4.55E-03
3	5.10E+09	2.14E+00	5.63E+03	1.50E-03	5.01E+09	1.56E-02	9.36E+08	8.33E-04
4	2.91E+00	1.60E+02	5.11E+03	5.58E-03	2.05E+06	7.80E+01	8.85E+08	1.36E-04
5	3.16E-07	9.62E+03	3.16E-07	1.93E+02	3.16E-07	8.11E+02	3.16E-07	2.28E+03
6	3.16E-06	3.63E+03	3.16E-06	1.93E+02	3.16E-06	1.10E+03	3.16E-06	5.07E+01
7	3.16E-05	1.55E+03	3.16E-05	4.76E+01	3.16E-05	8.95E+02	3.16E-05	5.09E+01
8	3.16E-04	7.26E+02	3.16E-04	1.45E+01	3.16E-04	4.32E+02	3.16E-04	1.82E+01
9	3.16E-03	6.79E+02	3.16E-03	3.19E+00	3.16E-03	5.94E+02	3.16E-03	3.64E+00
All mastics					Aggregate			
E_∞ (MPa)			μ		E(MPa)		μ	
3.16E-08			0.30		5.50E+04		0.25	

Table 4. Model Parameters for macroscale model

	0°C		50°C	
	E(MPa)	μ	*E*(MPa)	μ
Asphalt concrete				
Granodiorite	3.67E+04	0.3	5.76E+02	0.3
Limestone	2.51E+04		2.69E+02	
Dolomite	2.81E+04		4.15E+02	
Rhyolite	1.44E+04		6.63E+02	
MA5S layer	2.05E+04	0.35	1.05E+03	0.35
AC 16 BS	2.20E+04	0.35	1.11E+03	0.35
AC 32 TS	1.47E+04	0.35	1.23E+03	0.35
	E(MPa)		μ	
Base layer	1.20E+02		0.49	
Subgrade	4.50E+01		0.49	

In this study, two temperatures (0 °C and 50 °C) were specified in the simulation, and the performance of pavements, including load-bearing capacity, rutting resistance, and fatigue cracking resistance, were analyzed. Due to the lower rigidity of PA mixtures at high temperatures, the amplitudes of the load were specified as different values for the 0 °C and 50 °C simulations, which were 0.7 MPa and 0.0007 MPa, respectively. In addition, the tire loading was assigned to be constant (time=100 s) on the model to simulate the cumulative vehicle load.

3. Results and discussion

3.1. Load-bearing capacity of PA pavement

The deformations at pavement surface in the center of the loading area are shown in **Figure 3**, which reflects the load-bearing capacities of pavement at low and high temperatures.

At 0 °C, the pavement with Rhyolite filler immediately reached and stabilized at the largest value of deformation at a very early stage, and was subsequently exceeded by the pavements with the other three fillers, respectively. At the end of the loading time, the pavement with Dolomite filler had the highest deformation value at 0.293 mm. The second highest value appeared in the Limestone enhanced pavement, accounting for a deformation value of 0.272 mm. The deformations of the Granodiorite and Rhyolite

fillers enhanced pavements were 0.193 mm and 0.157 mm, respectively. Hence, this indicates that the capacity of Rhyolite filler enhanced pavement is the highest at the end of the loading period, followed by pavements with Granodiorite and Limestone fillers, and the pavement with Dolomite filler has the lowest capacities. In addition, the deformation of the pavements exhibited strong time-dependent properties. In particular, the Dolomite filler enhanced pavement showed the smallest value of deformation at early stages, and it gradually increased and eventually became the largest value at the end of loading, which is remarkably different from the pavement with Rhyolite filler. The distinction might be related to the viscoelastic properties of the PA mixture with different fillers. The PA mixture with Dolomite filler shows more viscous behavior at lower temperatures, and hence the responses were changing in the entire loading period; however, the PA mixture with Rhyolite filler exhibits more elasticity and responds to the loadings in an extremely short period. This different is believed to closely relate to the chemical components of the mineral filler, which will be discussed later.

At 50 °C, the deformations are much smaller than at 0 °C because the load amplitude is lower. All four PA pavements reach at their ultimate deformation values at very early stages, which can be ascribed to the lower rigidity of PA mixture at high temperatures. The Limestone enhanced PA pavement had the highest deformation value amongst the four filler types, followed by Dolomite and Granodiorite pavements, and Rhyolite pavement has the smallest deformation value. The deformation of Limestone and Dolomite enhanced pavements were 0.0231 mm and 0.0156 mm, respectively, more than three times of that of the Granodiorite (0.00494 mm) and Rhyolite (0.00427 mm) fillers. The results demonstrate that the load-bearing capacities of pavements with Granodiorite and Rhyolite fillers are close and much higher than the other two fillers at high temperatures. The Limestone filler enhanced pavement shows the smallest

capacity.

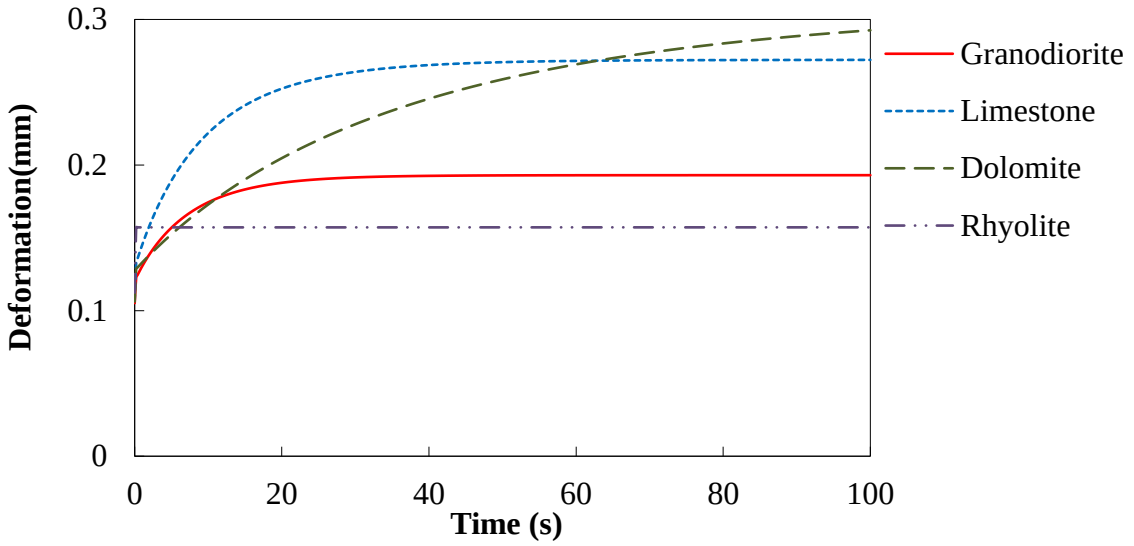

(a)

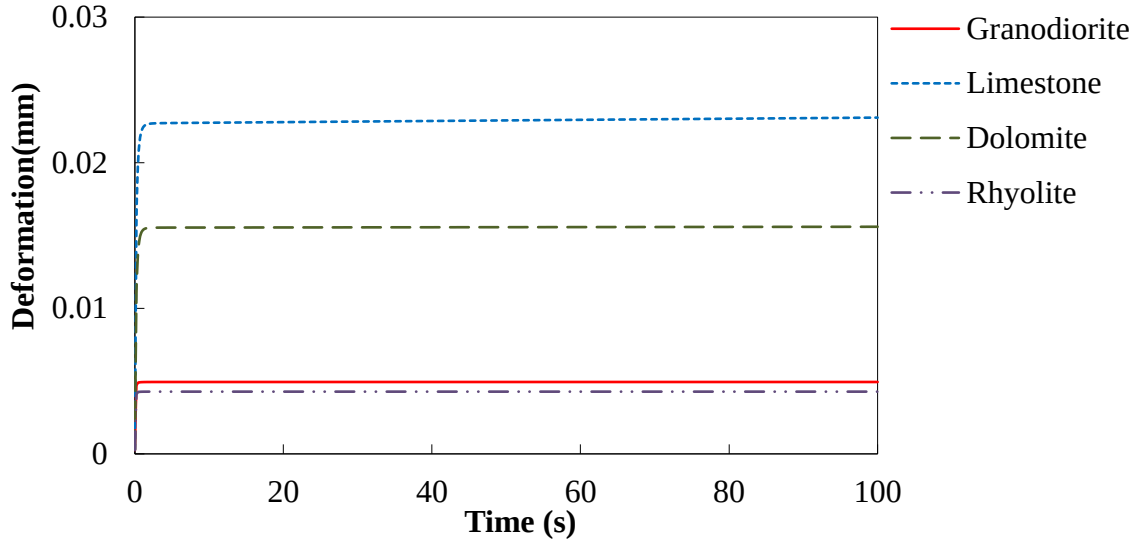

(b)

Figure 3. Image of deformation results: (a) 0°C;(b) 50°C

3.2. Rutting resistance of PA pavement at high temperature

The rutting resistance property of asphalt pavement can be predicted by the creep strain distribution. The rutting distress occurs in pavements when the creep strain is relatively higher. The location of the maximum creep strain is identical for the four

types of pavements with different fillers, and **Figure 4** exhibits the location of the maximum creep strain in pavement with Granodiorite filler at 50 °C.

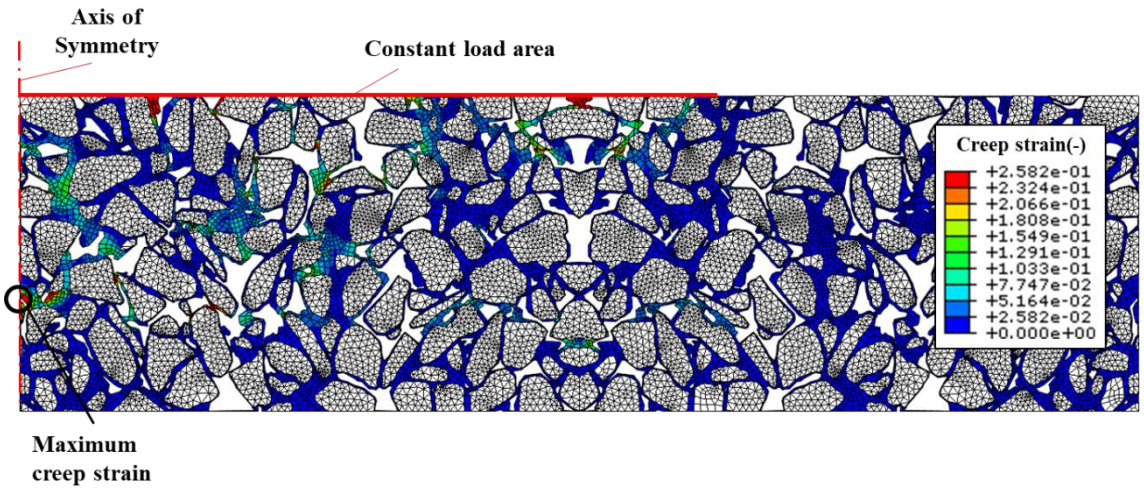

Figure 4. Image of the maximum creep strain location in pavement with Granodiorite filler at 50 °C

The maximum creep strain is located in the axis of symmetry, which is closely related to the rutting distress of pavements. The significant creep strains are mostly distributed under the loading area, especially near the surface of the pavement. Remarkable concentrations appear at the clearance between two aggregates, in which distresses can occur. The maximum creep strain values of the pavements with different fillers at 50 °C were calculated and illustrated in **Figure 5**.

The maximum creep strain of pavement with Dolomite filler has a relatively higher value than that with the other three fillers, indicating that the rutting distress would most probably initiate in this pavement. The smallest strain value appears in the Rhyolite enhanced PA pavement, which can be ascribed to the high capacity of this pavement.

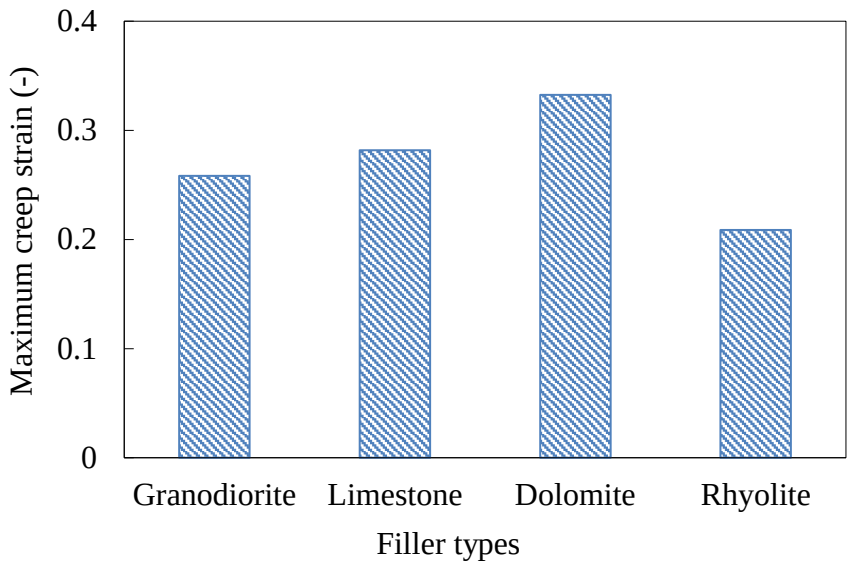

Figure 5. Image of the maximum creep strain at 50 °C

3.3. Raveling resistance of pavement at low temperature

The von Mises stress is used to demonstrate the raveling resistance of PA pavement at low temperatures (Zhang and Leng 2017). The higher von Mises stress values are caused by higher stress concentrations in which raveling distress can easily occur. Similarly, the von Mises stress distributions were identical for the pavements with the four mineral fillers. Hence, the von Mises stress distribution in the mastic of the pavement with Granodiorite filler at 0 °C is illustrated in **Figure 6**.

Within this figure, the remarkable von Mises stresses mostly distribute under the loading area, and the stress concentrations appear between two aggregates. Four specific positions with remarkable von Mises stress concentrations are selected as the critical positions for raveling distress. Particularly, the stress in position 2 is more significant than the other positions. The above results demonstrate that the raveling distress can occur in the small clearance of aggregate under the loading area in PA pavements, and position 2 is more vulnerable than the other positions in subjecting the cracking distress.

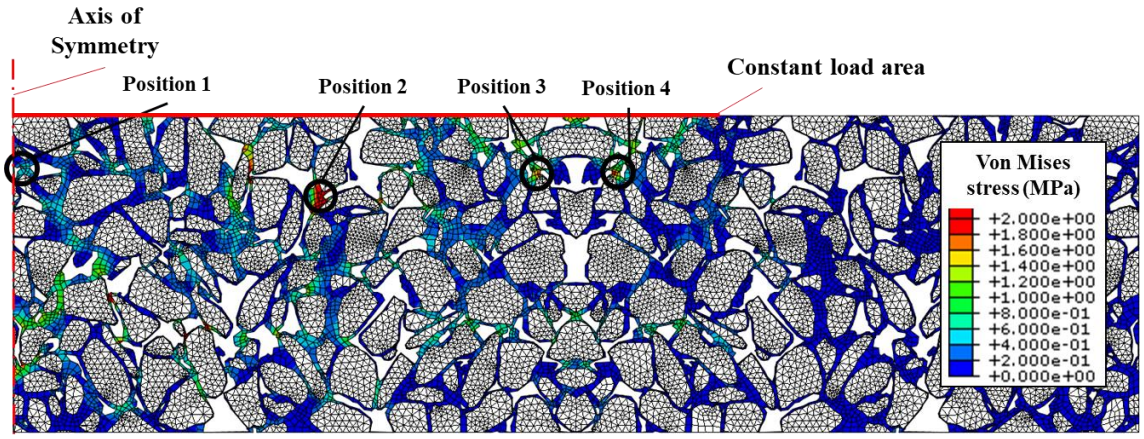

Figure 6. Image of critical locations of von Mises stress in pavement with Granodiorite filler at 0 °C

In addition, the mechanical responses of the pavements with different fillers exhibit significant time-dependent characterization, and therefore, the von Mises stress values for these four positions of PA pavements at various loading times are calculated and presented in **Figure 7**.

At the beginning of the loading (time=1s), the von Mises stress values of different fillers enhanced pavements derived from the same location are close to each other; furthermore, the maximum value of stress located in position 2 is much higher than the other three positions. The stress values in position 3 and position 4 are close, and position 1 has the smallest stress value in each pavement. Amongst the four different fillers, the highest and lowest stress values appear in pavements with Granodiorite and Rhyolite fillers, respectively, as shown in **Figure 7 (a)**.

As the loading time increases, the values of von Mises stress decrease especially for the pavements with Limestone and Dolomite fillers. At the end of the loading period (time=100s), the Rhyolite enhanced pavement had the largest von Mises stress, followed by Granodiorite, Limestone, and Dolomite fillers enhanced pavements. Moreover, the difference of stress at the four positions in pavement with Dolomite filler is smaller than that with the other three fillers, as shown in **Figure 7 (b)**.

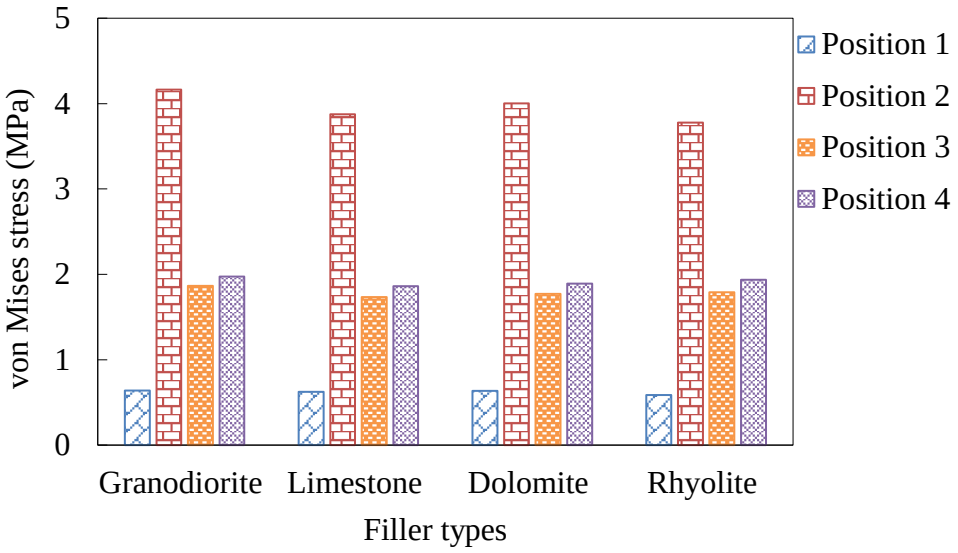

(a)

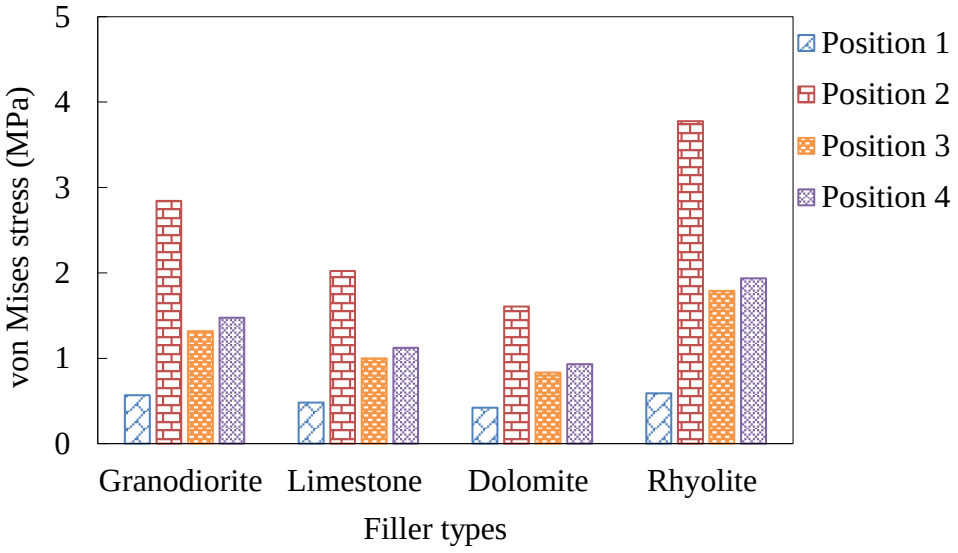

(b)

Figure 7. Values of von Mises stress in the pavement at 0°C: (a) Time=1s; (b) Time=100s.

At low temperatures, even though the mechanical behavior of PA mixture is close to the linear elastic, the responses to the cumulative tire loading exhibit remarkable time-dependent characteristic. The raveling resistances of pavements with fillers vary at different loading times. In the early stage of the loading period, the Rhyolite filler enhanced pavement has a relatively higher raveling resistance than others while that of

the Granodiorite filler enhanced pavement is lower. However, with an increase of the loading time, the von Mises stress values of the pavements decreased due to the stress relaxation of the PA mixture. In the later stage of the loading period, the pavements with Dolomite and Rhyolite respectively witnessed the highest and lowest raveling resistance. In addition, the small stress variation between the four positions in the pavement with Dolomite filler at the end of the loading time indicates that the Dolomite enhanced pavement becomes more flexible with an increase of the loading time, and thus has higher raveling resistance in the later stage of loading.

3.4. Performance ranking and correlation analysis

From the above simulation results, the performances of PA pavements with the four mineral fillers at low and high temperatures are identified. To make a comprehensive evaluation of the four filler types based on the PA pavement performance, a radar graph was employed in this study, as shown in **Figure 8**. The radar graph is structured such that an improvement in a material property can be expected with an increasing distance from the axis cross. Hence, the PA pavements with different fillers cover different areas in the diagram. In this study, four performances of PA pavement, namely load-bearing capacity at low temperature, load-bearing capacity at high temperature, rutting resistance at high temperature, and raveling resistance at low temperature, were evaluated. It should be noted that each of the three indexes (deformation, creep strain, and von Mises stress) has a negative correlation with the performance of pavements (load-bearing capacity, rutting resistance, and raveling resistance), and therefore, for each performance, the reciprocal of the index was calculated and analyzed.

It is illustrated that the pavements with Rhyolite and Granodiorite fillers show higher load-bearing capacity and rutting resistance, whilst the pavements with Dolomite and Limestone fillers have better raveling resistance. In conclusion, the PA mixtures

with Rhyolite and Granodiorite fillers are suitable for pavements under high temperature and standing heavy traffic, and the PA pavements with Limestone and Dolomite fillers have better anti-raveling performance.

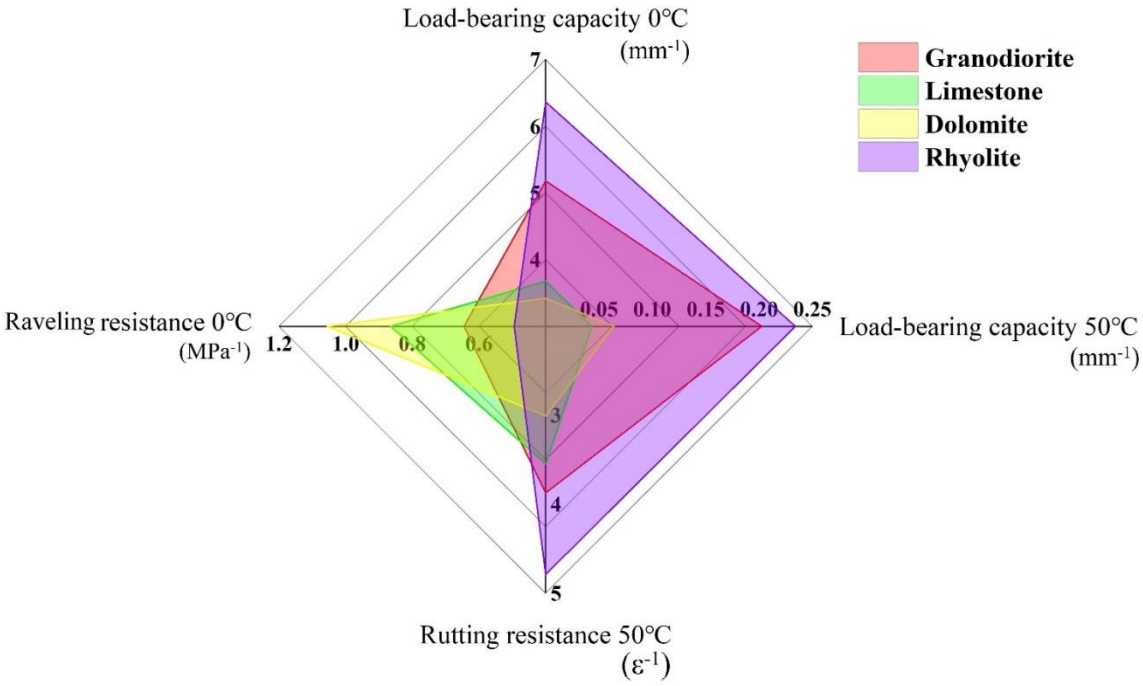

Figure 8. Diagram for the PA pavements with different fillers

In order to quantify the relationship between the chemical content of the mineral filler and the performance of each PA pavement, the Pearson correlation coefficients were calculated and listed in **Table 5**, which represents the linear relation between the two variables. The range of the coefficients is between -1.0 and 1.0, which respectively denotes the negative and positive correlation. When the coefficient values approach 0.0, the correlations between the two variables are weaker; a coefficient value of 0.0 denotes that there are no correlations between two variables.

Table 5. Pearson correlation coefficients

	Na_2O	MgO	Al_2O_3	SiO_2	K_2O	CaO	TiO_2	Fe_2O_3
Load-bearing capacity 0°C	0.614	-0.640	0.950	0.945	0.965	-0.884	0.418	0.538
Load-bearing capacity 50°C	0.776	-0.525	0.996	0.995	0.895	-0.976	0.602	0.735
Rutting resistance 50°C	0.427	-0.754	0.831	0.824	0.941	-0.710	0.237	0.316
Raveling resistance 0°C	-0.645	0.813	-0.917	-0.914	-0.884	0.798	-0.487	-0.537

It can be seen from **Table 5** that the components of Al_2O_3, SiO_2, K_2O, and CaO show the most significant relationships with the PA pavement performance. In addition, the chemical components of Na_2O, MgO, and Fe_2O_3 also exhibit strong relationships with some of the PA pavement performances. To clearly illustrate and compare the correlations, the Pearson correlation coefficients are presented in **Figure 9**. Within this figure, the components with coefficient values higher than 0.8 are regarded to have significant correlations, and the chain-dotted lines denote the coefficient values equal to 0.8 and -0.8.

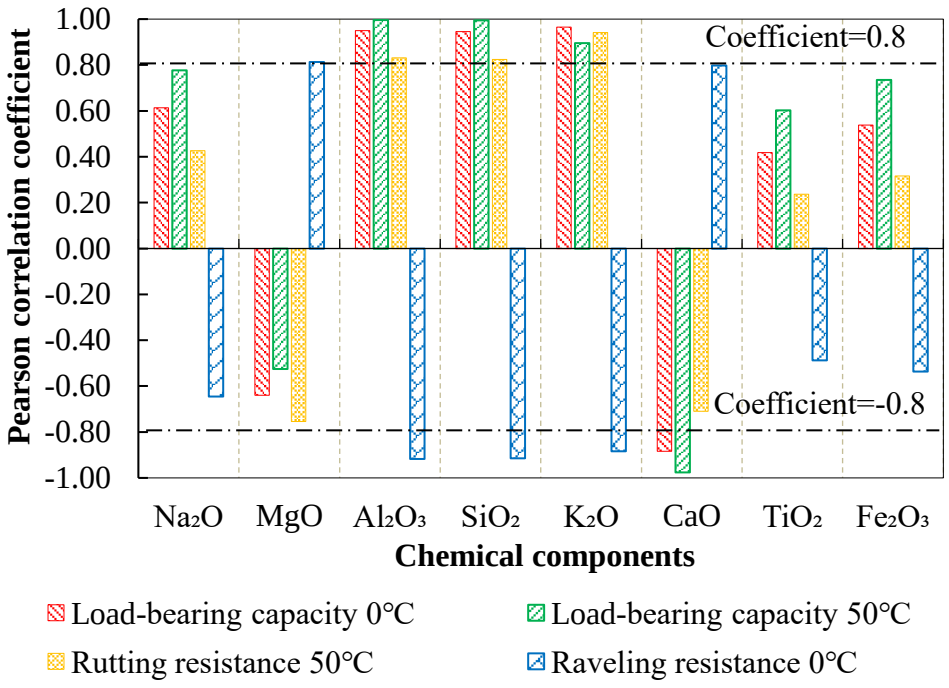

Figure 9. Image of Pearson correlation coefficients

It can be observed that the chemical components Na_2O, Al_2O_3, SiO_2, K_2O, TiO_2, and Fe_2O_3 exhibit positive correlations with the load-bearing capacity and rutting

resistance, and negative correlations with the raveling resistance of PA pavement. However, the mass components Na_2O, K_2O, TiO_2, and Fe_2O_3 are relatively small (much less than Al_2O_3 and SiO_2), and thus only the chemical components Al_2O_3 and SiO_2 are considered to play dominate roles in improving the load-bearing capacity and rutting resistance of PA mixtures as well as PA pavements.

On the other hand, the chemical components MgO and CaO show positive correlations with raveling resistance and negative correlations with load-bearing capacity and rutting resistance. The mass component as well as the correlation of CaO is much higher than that of MgO. Hence, it can be concluded that the fillers with high percentages of CaO can reduce the load-bearing capacity and rutting resistance of PA pavements, while the raveling resistance of PA pavements can be improved by increasing the CaO component.

4. Conclusions and outlook

The present study develops a coupled multiscale model to investigate the effects of mineral fillers on the performance of PA pavements. Within this model, the mesoscale model of a PA mixture was established from the CT image of the PA specimen based on DIP technology. Four types of asphalt mastic were prepared with different mineral fillers (Granodiorite, Limestone, Dolomite, and Rhyolite), and their linear viscoelastic properties at 0 °C and 50 °C were specified in the simulation. A constant loading was applied to the model to simulate cumulative tire loadings. As a result, the performances of the PA pavements with different fillers were obtained and ranked, and the correlations between pavement performance and the chemical components of fillers were identified.

(1) The heterogeneous structure of PA mixture causes significant stress or strain concentrations in mixture especially between two aggregate particles, which

makes it difficult to precisely predict the mechanical response of PA pavements.

(2) The pavements with Rhyolite and Granodiorite fillers have relatively higher load-bearing capacities under lower and higher temperatures.

(3) At high temperatures, the Rhyolite filler can more effectively improve the rutting resistance of PA pavement, while the pavement with Dolomite filler is more vulnerable when subjected to rutting distress.

(4) Although the properties of the PA mixtures are close to linear elasticity at low temperatures, remarkable time-dependent responses can still be observed in the deformation and von Mises stress distribution of pavements under accumulative loading. At the end of loading period, the pavement with Dolomite filler exhibits the best raveling resistance.

(5) The correlation analyses demonstrate that the components Al_2O_3 and SiO_2 can effectively improve the load-bearing capacities and rutting resistance of PA pavements, while the component CaO can enhance the raveling resistance of PA pavements.

The different mineral fillers significantly influence the mechanical response of the PA pavements. The abovementioned conclusions contribute to the current knowledge, and based on this algorithm, it is possible to select an optimal filler for a specific pavement design. However, only two temperatures (0 and 50 °C) were considered in the PA pavement simulations, and constant tire loading was applied to save the computational time. Further investigation needs to be carried out, for example, an intermedium temperature should be adopted in the FE simulation and the fatigue performance of the PA pavements should be simulated and evaluated.

References

Al-Hdabi, A., Al Nageim, H. & Seton, L., 2014. Performance of gap graded cold asphalt containing cement treated filler. *Construction and Building Materials,* 69,

362-369. http://doi.org/10.1016/j.conbuildmat.2014.07.081

Alber, S., Ressel, W., Liu, P., Hu, J., Wang, D., Oeser, M., Uribe, D. & Steeb, H., 2018. Investigation of microstructure characteristics of porous asphalt with relevance to acoustic pavement performance. *International Journal of Transportation Science and Technology,* 7 (3), 199-207. http://doi.org/10.1016/j.ijtst.2018.06.001

Allen, D.H., 2001. Homogenization principles and their application to continuum damage mechanics. *Composites Science and Technology,* 61 (15), 2223-2230. http://doi.org/10.1016/S0266-3538(01)00116-6

Allen, D.H., Little, D.N., Soares, R.F. & Berthelot, C., 2015. Multi-scale computational model for design of flexible pavement – part iii: Two-way coupled multi-scaling. *International Journal of Pavement Engineering,* 18 (4), 335-348. http://doi.org/10.1080/10298436.2015.1066001

Alvarez, A.E., Gomez, K.L., Gomez, D.C. & Reyes-Ortiz, O.J., 2019. Optimising the effect of natural filler on asphalt-aggregate interfaces based on surface free energy measurements. *Road Materials and Pavement Design,* 20 (7), 1548-1570. http://doi.org/10.1080/14680629.2018.1465451

Alvarez, A.E., Martin, A.E. & Estakhri, C., 2011. A review of mix design and evaluation research for permeable friction course mixtures. *Construction and Building Materials,* 25 (3), 1159-1166. http://doi.org/10.1016/j.conbuildmat.2010.09.038

Cardone, F., Frigio, F., Ferrotti, G. & Canestrari, F., 2015. Influence of mineral fillers on the rheological response of polymer-modified bitumens and mastics. *Journal of Traffic and Transportation Engineering (English Edition),* 2 (6), 373-381. http://doi.org/10.1016/j.jtte.2015.06.003

Dai, Q., Sadd, M.H., Parameswaran, V. & Shukla, A., 2005. Prediction of damage behaviors in asphalt materials using a micromechanical finite-element model and image analysis. *Journal of Engineering Mechanics,* 131 (7), 668-677. http://doi.org/10.1061/(asce)0733-9399(2005)131:7(668)

Du, C., Sun, Y., Chen, J., Gong, H., Wei, X. & Zhang, Z., 2020. Analysis of cohesive and adhesive damage initiations of asphalt pavement using a microstructure-based finite element model. *Construction and Building Materials,* 261, 119973. http://doi.org/10.1016/j.conbuildmat.2020.119973

Fgsv, 2007. Asphalt-stb, z. T. V. . *Zusätzliche Technische Vertragsbedingungen und Richtlinien für den Bau von Verkehrsflächenbefestigungen aus Asphalt.* Köln.

Fonseca, J.F., Teixeira, J., Branco, V. & Kim, Y.R., 2019. Evaluation of effects of filler by-products on fine aggregate matrix viscoelasticity and fatigue-fracture characteristics. *Journal of Materials in Civil Engineering,* 31 (10), 10. http://doi.org/10.1061/(asce)mt.1943-5533.0002891

Imaninasab, R., Bakhshi, B. & Shirini, B., 2016. Rutting performance of rubberized porous asphalt using finite element method (fem). *Construction and Building Materials,* 106, 382-391. http://doi.org/10.1016/j.conbuildmat.2015.12.134

Kim, Y.-R., Souza, F.V. & Teixeira, J.E.S.L., 2012. A two-way coupled multiscale model for predicting damage-associated performance of asphaltic roadways.

Computational Mechanics, 51 (2), 187-201. http://doi.org/10.1007/s00466-012-0716-8

Kim, Y.R. & Little, D.N., 2004. Linear viscoelastic analysis of asphalt mastics. *Journal of Materials in Civil Engineering,* 16 (2), 122-132. http://doi.org/10.1061/(asce)0899-1561(2004)16:2(122)

Klimczak, M. & Cecot, W., 2020. Synthetic microstructure generation and multiscale analysis of asphalt concrete. *Applied Sciences-Basel,* 10 (3), 11. http://doi.org/10.3390/app10030765

Kollmann, J., Lu, G., Liu, P., Xing, Q., Wang, D., Oeser, M. & Leischner, S., 2019. Parameter optimisation of a 2d finite element model to investigate the microstructural fracture behaviour of asphalt mixtures. *Theoretical and Applied Fracture Mechanics,* 103. http://doi.org/10.1016/j.tafmec.2019.102319

Li, X., Lv, X., Liu, X. & Ye, J., 2019. Discrete element analysis of indirect tensile fatigue test of asphalt mixture. *Applied Sciences,* 9 (2), 327. http://doi.org/10.3390/app9020327

Liu, P., Hu, J., Wang, H., Falla, G., Wang, D. & Oeser, M., 2018a. Influence of temperature on the mechanical response of asphalt mixtures using microstructural analysis and finite-element simulations. *Journal of Materials in Civil Engineering,* 30. http://doi.org/10.1061/(ASCE)MT.1943-5533.0002531

Liu, P., Wang, D., Hu, J. & Oeser, M., 2017. Safem – software with graphical user interface for fast and accurate finite element analysis of asphalt pavements. *Journal of Testing and Evaluation,* 45 (4), 1301-1315. http://doi.org/10.1520/JTE20150456

Liu, P., Xu, H., Wang, D., Wang, C., Schulze, C. & Oeser, M., 2018b. Comparison of mechanical responses of asphalt mixtures manufactured by different compaction methods. *Construction and Building Materials,* 162, 765-780. http://doi.org/10.1016/j.conbuildmat.2017.12.082

Liu, Q.T., Garcia, A., Schlangen, E. & Van De Ven, M., 2011. Induction healing of asphalt mastic and porous asphalt concrete. *Construction and Building Materials,* 25 (9), 3746-3752. http://doi.org/10.1016/j.conbuildmat.2011.04.016

Liu, Q.T., Schlangen, E., Van De Ven, M., Van Bochove, G. & Van Montfort, J., 2012. Evaluation of the induction healing effect of porous asphalt concrete through four point bending fatigue test. *Construction and Building Materials,* 29, 403-409. http://doi.org/10.1016/j.conbuildmat.2011.10.058

Lu, G.Y., Liu, P.F., Wang, Y.H., Fassbender, S., Wang, D.W. & Oeser, M., 2019a. Development of a sustainable pervious pavement material using recycled ceramic aggregate and bio-based polyurethane binder. *Journal of Cleaner Production,* 220, 1052-1060. http://doi.org/10.1016/j.jclepro.2019.02.184

Lu, G.Y., Renken, L., Li, T.S., Wang, D.W., Li, H. & Oeser, M., 2019b. Experimental study on the polyurethane-bound pervious mixtures in the application of permeable pavements. *Construction and Building Materials,* 202, 838-850. http://doi.org/10.1016/j.conbuildmat.2019.01.051

Manrique-Sanchez, L. & Caro, S., 2019. Numerical assessment of the structural

contribution of porous friction courses (pfc). *Construction and Building Materials,* 225, 754-764. http://doi.org/10.1016/j.conbuildmat.2019.07.200

Mohd Shukry, N.A., Abdul Hassan, N., Abdullah, M.E., Hainin, M.R., Yusoff, N.I.M., Mahmud, M.Z.H., Putra Jaya, R., Warid, M.N.M. & Mohd Satar, Mohd k.I., 2018. Influence of diatomite filler on rheological properties of porous asphalt mastic. *International Journal of Pavement Engineering,* 21 (4), 428-436. http://doi.org/10.1080/10298436.2018.1483504

Qian, N., Wang, D., Li, D. & Shi, L., 2020. Three-dimensional mesoscopic permeability of porous asphalt mixture. *Construction and Building Materials,* 236. http://doi.org/10.1016/j.conbuildmat.2019.117430

Reyes-Ortiz, O.J., Mejia, M. & Useche-Castelblanco, J.S., 2019. Aggregate segmentation of asphaltic mixes using digital image processing. *Bulletin of the Polish Academy of Sciences-Technical Sciences,* 67 (2), 279-287. http://doi.org/10.24425/bpas.2019.128115

Rieksts, K., Pettinari, M. & Haritonovs, V., 2018. The influence of filler type and gradation on the rheological performance of mastics. *Road Materials and Pavement Design,* 20 (4), 964-978. http://doi.org/10.1080/14680629.2018.1428216

Roberto, A., Romeo, E., Montepara, A. & Roncella, R., 2020. Effect of fillers and their fractional voids on fundamental fracture properties of asphalt mixtures and mastics. *Road Materials and Pavement Design,* 21 (1), 25-41. http://doi.org/10.1080/14680629.2018.1475297

Rochlani, M., Leischner, S., Falla, G.C., Wang, D., Caro, S. & Wellner, F., 2019. Influence of filler properties on the rheological, cryogenic, fatigue and rutting performance of mastics. *Construction and Building Materials,* 227. http://doi.org/10.1016/j.conbuildmat.2019.116974

Schapery, R.A., 1981. On viscoelastic deformation and failure behavior of composite materials with distributed flaws. *Advances in aerospace structures materials and design*, 5-20.

Shafabakhsh, G., Kashi, E. & Tahani, M., 2018. Analysis of runway pavement response under aircraft moving load by fem. *Journal of Engineering, Design and Technology,* 16 (2), 233-243. http://doi.org/10.1108/JEDT-09-2017-0093

Stewart, C.M. & Garcia, E., 2019. Fatigue crack growth of a hot mix asphalt using digital image correlation. *International Journal of Fatigue,* 120, 254-266. http://doi.org/10.1016/j.ijfatigue.2018.11.024

Sun, Y., Du, C., Gong, H., Li, Y. & Chen, J., 2020. Effect of temperature field on damage initiation in asphalt pavement: A microstructure-based multiscale finite element method. *Mechanics of Materials,* 144, 103367. http://doi.org/10.1016/j.mechmat.2020.103367

Sun, Y., Du, C., Zhou, C., Zhu, X. & Chen, J., 2019. Analysis of load-induced top-down cracking initiation in asphalt pavements using a two-dimensional microstructure-based multiscale finite element method. *Engineering Fracture Mechanics,* 216, 106497. http://doi.org/10.1016/j.engfracmech.2019.106497

Tschoegl, N.W., 2012. *The phenomenological theory of linear viscoelastic behavior: An introduction*: Springer Science & Business Media.

Wang, H., Wang, J. & Chen, J., 2014. Micromechanical analysis of asphalt mixture fracture with adhesive and cohesive failure. *Engineering Fracture Mechanics,* 132, 104-119. http://doi.org/10.1016/j.engfracmech.2014.10.029

Wollny, I., Hartung, F., Kaliske, M., Liu, P., Oeser, M., Wang, D., Canon Falla, G., Leischner, S. & Wellner, F., 2020. Coupling of microstructural and macrostructural computational approaches for asphalt pavements under rolling tire load. *Computer-Aided Civil and Infrastructure Engineering*. http://doi.org/10.1111/mice.12535

Xing, C., Xu, H.N., Tan, Y.Q., Liu, X.Y., Zhou, C.H. & Scarpas, T., 2019. Gradation measurement of asphalt mixture by x-ray ct images and digital image processing methods. *Measurement,* 132, 377-386. http://doi.org/10.1016/j.measurement.2018.09.066

Yin, A., Yang, X., Gao, H. & Zhu, H., 2012. Tensile fracture simulation of random heterogeneous asphalt mixture with cohesive crack model. *Engineering Fracture Mechanics,* 92, 40-55. http://doi.org/10.1016/j.engfracmech.2012.05.016

Zhang, D., Gu, L. & Zhu, J., 2019. Effects of aggregate mesostructure on permanent deformation of asphalt mixture using three-dimensional discrete element modeling. *Materials (Basel),* 12 (21). http://doi.org/10.3390/ma12213601

Zhang, Y. & Leng, Z., 2017. Quantification of bituminous mortar ageing and its application in ravelling evaluation of porous asphalt wearing courses. *Materials & Design,* 119, 1-11. http://doi.org/10.1016/j.matdes.2017.01.052

Zhang, Y., Van De Ven, M., Molenaar, A. & Wu, S., 2016. Preventive maintenance of porous asphalt concrete using surface treatment technology. *Materials & Design,* 99, 262-272. http://doi.org/10.1016/j.matdes.2016.03.082

Ziaei-Rad, V., Nouri, N., Ziaei-Rad, S. & Abtahi, M., 2012. A numerical study on mechanical performance of asphalt mixture using a meso-scale finite element model. *Finite Elements in Analysis and Design,* 57, 81-91. http://doi.org/10.1016/j.finel.2012.03.004